J Electroceram (2010) 24:15–19
DOI 10.1007/s10832-008-9435-0

# Nanoscale engineering of ferroelectric functionality

**M. Tyunina · I. Jaakola · M. Plekh · J. Levoska**

Received: 28 September 2007 / Accepted: 24 January 2008 / Published online: 13 February 2008


**Abstract** In epitaxial films of perovskite ferroelectrics, functionality can be controlled by size-strain-surface effects. Experimental evidence of such a possibility is demonstrated in epitaxial heterostructures of $BaTiO_3$ thin films and of (Ba,Sr)$TiO_3$ superlattices grown by pulsed laser deposition on $La_{0.5}Sr_{0.5}CoO_3$/MgO (001). In epitaxial $BaTiO_3$ films, temperature of phase transition is shown to be a function of in-plane biaxial strain and film thickness. In epitaxial (Ba,Sr)$TiO_3$ superlattices, the dielectric permittivity, tunability, and temperature of phase transition are shown to be a function of strain and superlattice period. The technological and principal problems limiting nanoscale engineering of ferroelectric functionality are also discussed.

**Keywords** Perovskite · Ferroelectric · Epitaxial · Functionality

## 1 Introduction

$ABO_3$-type perovskites (such as $BaTiO_3$, $KNbO_3$, etc.) exhibit ferroelectric (FE) behaviour. Spontaneous polarization that can be switched by applying electric field and presence of polarization domains are characteristic features of FEs. In FEs, several effects (pyroelectric, piezoelectric, electrooptic, piezooptic, electrocaloric, etc.) coexist, with a strong dependence of properties on temperature and applied field. This makes FEs functional and smart, and enables versatile device applications of these materials in crystal or ceramic form [1]. Devices employing FE in thin-film form such as memories, field-effect transistors, tunable capacitors, and sensors have been demonstrated too [2, 3].

In bulk crystals and ceramics, FE functionality can be engineered by A-site and/or B-site doping in $(A^1,A^2)(B^1,B^2)O_3$, by formation of solid solutions of two or more perovskite FEs $(1-x)A^1B^1O_{3-}(x)A^2B^2O_3$, by controlling domain and/or domain wall configuration, and by controlling grain size and/or grain design (e.g. core-shell structured grains) in ceramics.

In epitaxial thin films grown on dissimilar substrates, another approach to engineering FE functionality is possible due to mismatch strain and clamping [4–7]. When FE film grows on a single-crystal substrate, both in-plane (parallel to the substrate surface) and out-of-plane (normal to the substrate surface) lattice parameters of the film, *a* and *c* for simplicity, are "adjusted" to the microstructure and thermophysical properties of the substrate [8]. Also structural phase transitions in the film are restricted by the presence of the substrate. Temperature–strain phase diagram of thin-film FE considerably differs from the phase diagram of the bulk prototype. In epitaxial perovskite films with nanometer-scale thickness, new structural and FE phases can exist, temperatures of phase transitions depend on strain *s*, and polarization can be enhanced by strain [4–7, 9]. This gives principal possibility for engineering FE functionality by controlling strain effects.

M. Tyunina (✉) · I. Jaakola · M. Plekh · J. Levoska
Microelectronics and Materials Physics Laboratories,
University of Oulu,
Oulu PL 4500,
90014 Oulun Yliopisto, Finland
e-mail: marinat@ee.oulu.fi

## 2 Strain and functionality in epitaxial $BaTiO_3$ films

To experimentally demonstrate such a possibility, epitaxial heterostructures of 20–400 nm thick films of $BaTiO_3$ (BTO) with an oxide $La_{0.5}Sr_{0.5}CoO_3$ (LSCO) bottom

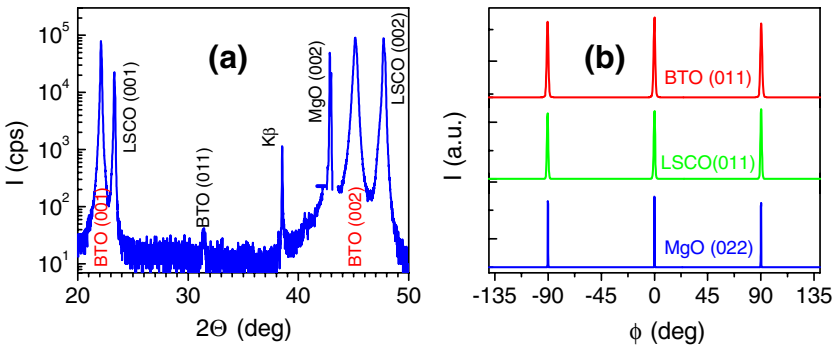


**Fig. 1** (**a**) $\Theta - 2\Theta$ XRD pattern of BTO/LSCO/MgO heterostructure. Only (00*l*) planes are seen. (**b**) ϕ-scans around (011)BTO, (011)LSCO, and (022)MgO. Epitaxial cube-on-cube growth is confirmed

electrode layers and Pt top electrodes were grown on MgO (001) single-crystal substrates by *in situ* pulsed laser deposition at BTO growth temperature of 1073 K. The room-temperature X-ray diffraction studies showed that BTO films were perovskite, with a pseudocubic crystal structure, oriented with (001) planes parallel to the substrate (001) surface Fig. 1(a). An in-plane epitaxial relationship Fig. 1(b) was BTO [100](001) || LSCO [100](001) || MgO [100](001). The out-of-plane lattice parameters *c* were determined from the $\Theta$–$2\Theta$ scans of (004) reflections and the in-plane parameters *a*—from the combination of (004) and (024) reflections. The BTO lattice parameters Fig. 2(a) and tetragonality *c*/*a* [Fig. 2(b)] appeared to be thickness dependent. The in-plane biaxial strain *s* in the main part of BTO films was found [10] to be compressive and also thickness dependent [Fig. 2(b)].

The impedance of the vertical LSCO/BTO/Pt capacitor heterostructures was measured using an HP 4284 *LCR*-meter, and the real part $\varepsilon$ of the relative dielectric permittivity in the BTO heterostructures was found using impedance analysis [11]. The temperature $T_m$ of the dielectric maximum indicating the phase transition was a function of both the in-plane strain Fig. 3(a) and BTO thickness *d* Fig. 3(b). Increase of $T_m$ with increasing compressive strain *s* was in agreement with the modelling [4–7]. In the studied range of $T$>77 K, dielectric maximum could not be detected for $d$<40 nm, evidencing the effect of internal field [12, 13]. The obtained considerable shift of $T_m$ to higher $T$ at even rather weak in-plane strain confirms the possibility to engineer FE functionality by strain.

## 3 Strain and functionality in epitaxial (Ba,Sr)$TiO_3$ superlattices

Previously, shift of $T_m$ by 500 K and huge enhancement of out-of-plane polarization have been demonstrated [9] in tetragonal BTO films with strong in-plane compression provided by coherent growth on specially selected $DyScO_3$ substrates with the lattice parameters close to that of BTO. However generally in epitaxial heterostructures, strain engineering is limited by strain relaxation through formation of misfit dislocations. In FE epitaxial films with a moderate lattice misfit between film and substrate, a pseudomorphic strained region with critical thickness of few nanometers is formed near the substrate, with a misfit dislocation arrangement between this region and a relaxed region. On the other side, large unrelaxed strain can be accumulated in superlattices [14–16] of two or more constituents with slightly different lattice parameters, and with thickness of each layer smaller than the critical one. In perovskite FE superlattices additionally to strain, also electrostatic coupling between the layers can influence functionality [17–19].

Here in attempt to obtain enhancement of dielectric permittivity and nonlinearity, epitaxial superlattices were

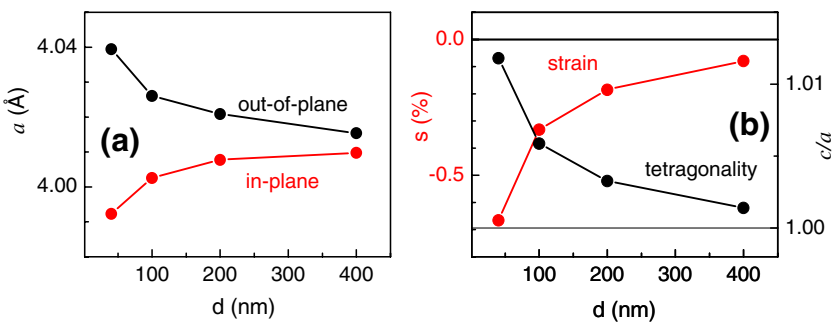


**Fig. 2** (**a**) Out-of-plane and in-plane lattice parameters in epitaxial films of BTO as a function of film thickness *d*. (**b**) Tetragonality *c*/*a* and in-plane strain *s* in epitaxial films of BTO as a function of film thickness *d*

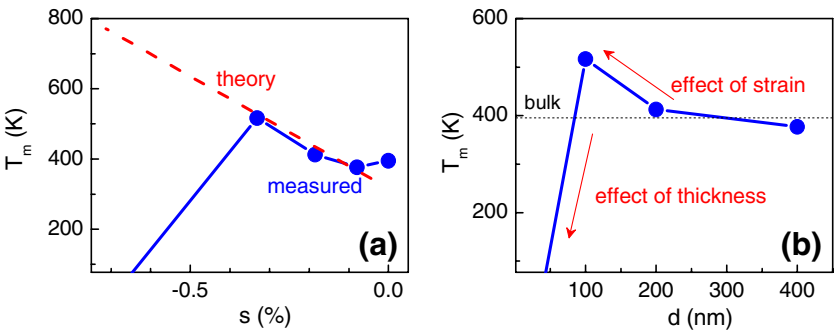


**Fig. 3** (**a**) Temperature of dielectric maximum $T_m$ as a function of strain $s$ in heterostructures of BTO/LSCO/MgO with different BTO film thickness. (**b**) Temperature of dielectric maximum $T_m$ as a function of BTO film thickness $d$ in BTO/LSCO/MgO heterostructures with different strain

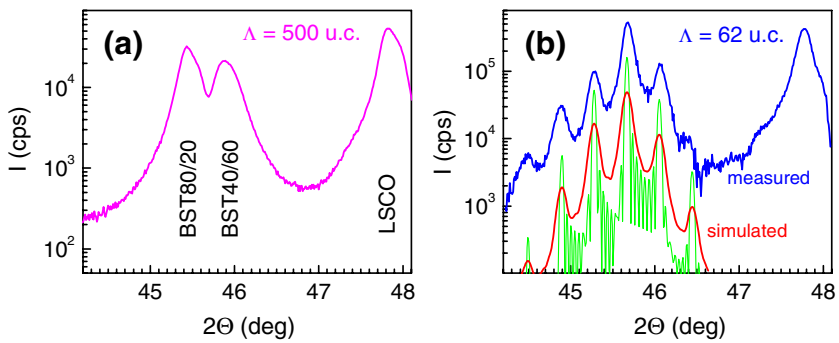


**Fig. 4** (**a**) $\Theta - 2\Theta$ scan around perovskite (002) reflection in (**a**) BST multilayer with period 500 u.c. and in (**b**) BST superlattice

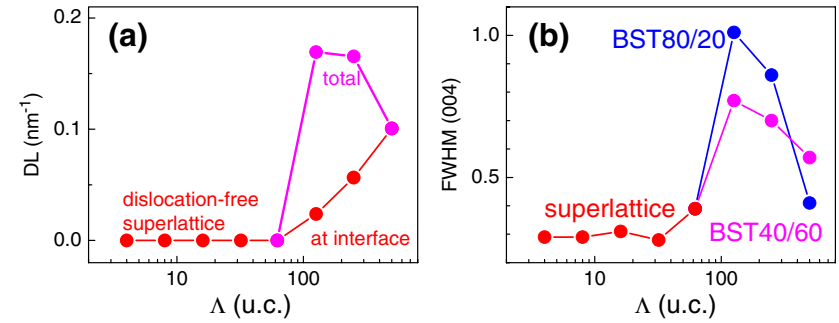


**Fig. 5** (**a**) Length of misfit dislocations at BST interface and the total length in the heterostructure as a function of period Λ. Superlattices are free of dislocations. (**b**) FWHM of (004) perovskite reflection as a function of period Λ

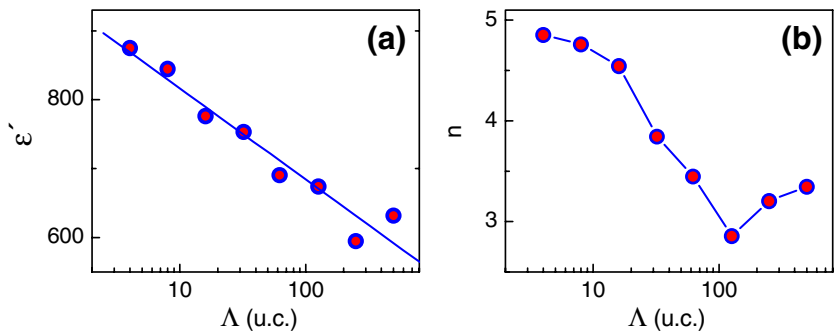


**Fig. 6** The room-temperature (**a**) permittivity $\varepsilon$ and (**b**) tunability $n$ as a function of period Λ in BST/LSCO/MgO heterostructures. Frequency $f$=20 kHz

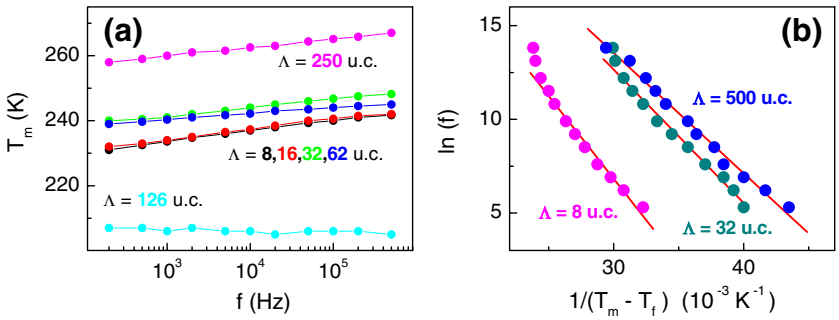


**Fig. 7** (**a**) Temperature $T_m$ as a function of frequency $f$ and (**b**) fit to the Vogel–Fulcher relationship in BST/LSCO/MgO heterostructures

formed using $Ba_{0.8}Sr_{0.2}TiO_3$ (BST80/20) and $Ba_{0.4}Sr_{0.6}TiO_3$ (BST40/60) as constituents. The mismatch between bulk lattice parameters of BST80/20 and BST40/60 is about 1.0%, allowing growth of BST superlattice with relatively large layer thicknesses and an estimated in-plane biaxial strain of 0.5% (compressive in BST80/20 and tensile in BST40/60). The number of pairs of BST layers with similar thickness in BST/LSCO/MgO stacks and the thickness of each layer were varied keeping the total thickness of the BST stack equal to 200 nm. Period Λ was changed from 1.6 nm, or 4 unit cells (u.c.) to 200 nm, or 500 u.c.

The formation of superlattices with a coherent pseudomorphic growth of BST layers was revealed for period $\Lambda \leq$ 62 u.c. This was evidenced [20] by presence of satellite peaks in $\Theta$–$2\Theta$ XRD patterns Fig. 4 and in reciprocal space maps, and by similarity of in-plane lattice parameters in all BST layers. The level of biaxial in-plane strain $s$ achieved in superlattice constituents is about $s \approx -0.4\%$ (compressive) in BST80/20 and $s \approx 0.3\%$ (tensile) in BST40/60.

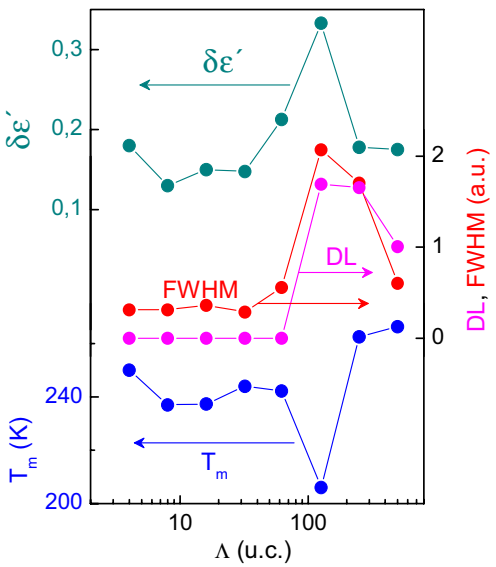


**Fig. 8** Correlation between structural and dielectric properties in BST/LSCO/MgO heterostructures. Temperature $T_m$, frequency dispersion of permittivity $\delta\varepsilon$, length of dislocations DL, and FWHM of (004) perovskite reflection as a function of period Λ

At the interface between BST layers, the length of dislocations per unit area DL was estimated, with the total dislocation length being characterized by DL×$N$, where $N$ is the number of interfaces. The maximum total DL is found for $L$=126 u.c., while superlattices are free of dislocations and strain relaxation [Fig. 5(a)] that is evidenced also by a decrease of the FWHM of the (004) reflections in $\Theta$–$2\Theta$ scans [Fig. 5(b)].

In all BST heterostructures, both the room-temperature permittivity $\varepsilon$ Fig. 6(a) and tunability $n$ Fig. 6(b) increase with decreasing period Λ. The tunability $n$ is determined as $n = \varepsilon(0)/\varepsilon(7\,\mathrm{V})$, where $\varepsilon(0)$ and $\varepsilon(7\ \mathrm{V})$ is the permittivity measured at zero biasing voltage and that measured at the bias of 7 V, respectively. To understand the mechanism responsible for the increase, the dielectric behaviour was studied in more details.

Analysis of the permittivity as a function of temperature and frequency revealed a frequency dependent $T_m(f)$ tending to decrease with decreasing Λ (for $\Lambda \neq 126$ u.c.) Fig. 7(a). Also for $\Lambda \neq 126$ u.c., a good linear fit to $\ln(f) \propto 1/(T_m - T_f)$ was obtained Fig. 7(b) evidencing the validity of the empirical Vogel–Fulcher relationship between measurement frequency $f$ and temperature $T_m$ of dielectric maximum: $f = f_0 \exp\{-E_A/[k_B(T_m - T_f)]\}$. Here $k_B$ is the Boltzmann constant and $f_0$, $E_A$, and $T_f$ are fitting parameters. The observed Vogel–Fulcher law and additional studies of the high-temperature and nonlinear behaviour [21] show that in the range of more than 400 K around $T_m$,

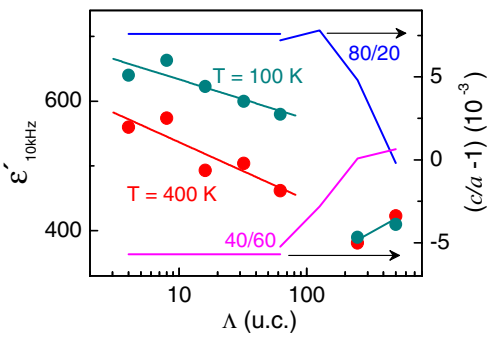


**Fig. 9** The permittivity $\varepsilon$ of BST heterostructures and tetragonality $c/a$ of constituents as a function of period Λ

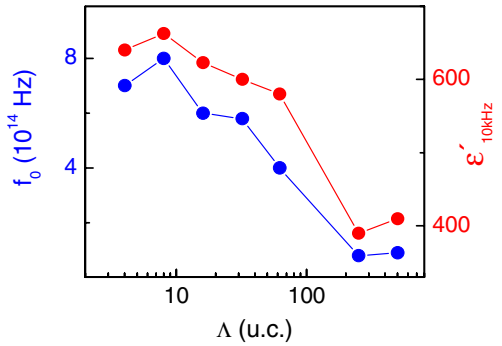


**Fig. 10** The room-temperature permittivity $\varepsilon$ and the frequency $f_0$ obtained from the Vogel–Fulcher fit as a function of period $\Lambda$

the heterostructures exhibit glasslike (GL) behaviour resembling that in thin-film relaxors and also that recently detected in thin-film $BaTiO_3$ [10].

It should be noted that in the multilayer with $\Lambda$=126 u.c., the lowest and frequency independent $T_m$ is observed, with the strongest frequency dispersion of permittivity $\delta\varepsilon=(\varepsilon_{200Hz}-\varepsilon_{1MHz})/\varepsilon_{200Hz}$, and with peculiarities in the dielectric nonlinearity. These anomalies are in a good agreement with the largest FWHM and the largest total dislocation length DL at $\Lambda$=126 u.c. [Fig. 8]. This allows ascribing the dielectric peculiarities in the multilayer with $\Lambda$=126 u.c. to a large volume of the dislocation-rich material in the BST stack.

In BST superlattices, the dielectric permittivity $\varepsilon$ is larger than that in BST multilayers. This can principally be ascribed to the larger strain in BST layers achieved in superlattices. However, with decreasing $\Lambda\leq$62 u.c. the permittivity $\varepsilon$ continues to increase [Fig. 9], while strain and tetragonality $c/a$ in the layers remain unchanged. Such an increase is observed at all temperatures. Thus the strain alone can hardly be responsible for the permittivity evolution.

Probably for understanding the permittivity increase, also the glasslike behaviour of BST and dynamic character of the measured permittivity $\varepsilon(f,T)$ should be taken into consideration, i.e.:

$$\varepsilon(f,T)=\varepsilon_s\int_{\tau_{\min}}^{1/f}G(\ln\tau,T)d\tau, \qquad (1)$$

where $\varepsilon_s$ is the static permittivity and $G(\ln\tau,T)$ is the relaxation time spectrum. As follows from the Vogel–Fulcher analysis, with decreasing $\Lambda$ the relaxation time spectra change. An obvious correlation between $f_0(\Lambda)$ and $\varepsilon(\Lambda)$ [Fig. 10] indicates that evolution of $G$ can be responsible for the permittivity increase. Thus system dynamics can be an important factor contributing to functionality in epitaxial superlattices of BST.

## 4 Conclusions

In epitaxial films of perovskite FEs, FE functionality can be controlled by size-strain-surface effects. Nanoscale engineering of functionality is possible. Experimental evidence of such a possibility is demonstrated. In epitaxial $BaTiO_3$ films, temperature of phase transition is shown to be a function of in-plane biaxial strain and film thickness. In epitaxial $(Ba,Sr)TiO_3$ superlattices, the dielectric permittivity, tunability, and temperature of phase transition are shown to be a function of strain and superlattice period. Along with successful engineering of functionality, also the technological and principal problems are shown, namely: unwanted effects of dislocations and interfaces, and possible contribution of the dynamic effects.

**Acknowledgments** Authors acknowledge Graduate School in Electronics, Telecommunications and Automation (I.J.), Infotech Oulu Graduate School (M.P.), Academy of Finland (project no 118250), and EU FP6 (project no 027468) for financial support.

## References

1. K. Uchino, *Ferroelectric Devices* (Marcel Dekker, New York, Basel, 2000), p. 308, ISBN 0-8247-8133-3
2. M. Dawber, K.M. Rabe, J.F. Scott, Rev. Mod. Phys. **77**, 1083 (2005) and references therein
3. N. Setter et al., J. Appl. Phys. **100**, 051606 (2006)
4. N.A. Pertsev, A.G. Zembilgotov, A.K. Tagantsev, Phys. Rev. Lett. **80**, 1988 (1998)
5. N.A. Pertsev, V.G. Koukhar, Phys. Rev. Lett. **84**, 3722 (2000)
6. V.G. Koukhar, N.A. Pertsev, R. Waser, Phys. Rev. B **64**, 214103 (2001)
7. O. Dieguez, S. Tinte, A. Antons, C. Bungaro, J.B. Neaton, K.M. Rabe, D. Vanderbilt, Phys. Rev. B **69**, 212101 (2004)
8. J.S. Speck, W. Pompe, J. Appl. Phys. **76**, 466 (1994)
9. K.J. Choi et al., Science **306**, 1005 (2004)
10. M. Tyunina, J. Levoska, I. Jaakola, Phys. Rev. B **75**, 140102(R) (2007)
11. M. Tyunina, J. Phys. Condens. Matter **18**, 5725 (2006)
12. M.D. Glinchuk, A.N. Morozovska, J. Phys. Condens. Matter **16**, 3517 (2004)
13. M.D. Glinchuk, A.N. Morozovska, E.A. Eliseev, J. Appl. Phys. **99**, 144102 (2006)
14. H. Tabata, H. Tanaka, T. Kawai, Appl. Phys. Lett. **65**, 1970 (1994)
15. T. Shimuta, O. Nakagawara, T. Makino, S. Arai, H. Tabata, T. Kawai, J. Appl. Phys. **91**, 2290 (2002)
16. H.N. Lee, H.M. Christen, M.F. Chisholm, C.M. Rouleau, D.H. Lowndes, Nature (London) **433**, 395 (2005)
17. A.L. Roytburd, S. Zhong, S.P. Alpay, Appl. Phys. Lett. **87**, 092902 (2005)
18. V.A. Stephanovich, I.A. Luk, yanchuk, M.G. Karkut, Phys. Rev. Lett. **94**, 047601 (2005)
19. K. Johnston, X. Huang, J.B. Neaton, K.M. Rabe, Phys. Rev. B **71**, 100103(R) (2005)
20. I. Jaakola, J. Levoska, M. Tyunina, J. Appl. Phys. **102**, 014108 (2007)
21. M. Tyunina, I. Jaakola, J. Levoska, M. Plekh, Phys. Rev. B **76**, 134107 (2007)